PERGAMON

International Journal of Multiphase Flow 26 (2000) 531–547

International Journal of Multiphase Flow

www.elsevier.com/locate/ijmulflow

Evaporation waves in flashing processes

E. Hahne*, G. Barthau

Institut für Thermodynamik und Wärmetechnik, University Stuttgart, Pfaffenwaldring 6, D-70550 Stuttgart, Germany

Received 14 April 1998; received in revised form 23 April 1999

Abstract

An experimental study on the inception and propagation of evaporation waves in adiabatic flashing of Refrigerant 11 has been performed in glass tubes with diameters $32\ \text{mm} \leq d \leq 252\ \text{mm}$. The formation of evaporation waves was observed at superheats $35\ \text{K} \leq \Delta\vartheta_{\max} \leq 50\ \text{K}$ and at depressurization rates as low as $\Delta p/\Delta t \approx 1$ bar/s. Additional experiments with metallic inserts as starters in the test tubes indicate, that the presence of metal/liquid contacts decreases the necessary superheat for the formation of evaporation waves and increases the propagation velocity of the wave along the metallic surface into the superheated liquid.

Keywords: Depressurization; Flashing; Evaporation wave; Boiling front; Metastable (superheated) liquid; Homogeneous two-phase flow; Refrigerant 11

1. Introduction

When a pressurized liquid in equilibrium with its vapor in a closed container is suddenly depressurized from the vapor side, the whole bulk of the liquid becomes superheated (metastable) with respect to the decreasing pressure, and adiabatic flashing will occur. Such flashing processes can occur either intentionally, e.g., in steam accumulators, or undesiredly, e.g., during blowdown in chemical reactors or due to pipe fracture in liquefied-gas containers. The governing parameters for the resulting thermo-hydraulic processes are: the amount of pressure decay and the depressurization rate. In steam accumulators, the depressurization rate

* Corresponding author. Tel.: +49-711-685-3536; fax: +49-711-685-3503.
E-mail address: pm@itw.uni-stuttgart.de (E. Hahne).

0301-9322/00/$ - see front matter
PII: S0301-9322(99)00031-2

is in the range of some bar/h, whereas in a guillotine break of large pipes, depressurization rates of up to Mbar/s can occur.

The unique characteristic of such adiabatic flashing processes is the withdrawal of the latent heat of evaporation from the internal energy of the superheated liquid. By its very definition, a phase change process is bound to an interface; consequently the intensity of the process is limited either by transport of energy to this interface, or by transport of the interface to the energy, or by the formation of new interfaces near the energy supply. Therefore, extent and distribution of liquid/vapor interfaces in the system are of paramount importance for the intensity of evaporation in flashing processes.

Most experimental studies concerning the depressurization of saturated or slightly subcooled liquids in containers deal with secondary effects, i.e., pressure–time variation, two-phase level swell, vapor separation or two-phase discharge.

As primary effects we consider: formation, distribution and propagation of liquid/vapor interfaces in the superheated liquid, since these are necessary initial conditions for modeling the flashing process. In existing models for flashing processes, it is often postulated that heterogeneous or homogeneous nucleation with classical bubble growth occurs. Respective equations use empirical adjustment parameters, to fit in with the experimental data (Kendoush, 1989; Bartak, 1990; Deligiannis and Cleaver, 1992; Elias and Chambre, 1993; Akyuzlu, 1993; Boesmans and Berghmans, 1994; Deligiannis and Cleaver, 1996).

There is, however, clear evidence that a totally different phenomenon — namely an evaporation wave — can occur also in a flashing process (Grolmes and Fauske, 1974; Viecenz, 1980; Chaves, 1984; Lund, 1986; Thompson et al., 1987; Hill and Sturtevant, 1989; Shepherd et al., 1989; Reinke and Yadigaroglu, 1995).

The phenomenon can be explained as follows: When the pressure decay is not high enough to initiate homogeneous nucleation within the liquid and when the container walls do not offer nucleation sites for heterogeneous nucleation on arbitrary sites, the phase change process is necessarily restricted to the liquid level. At a given threshold superheat (depending on depressurization rate), the original smooth liquid level undergoes an instability which rapidly spreads over the entire surface, generating a jet of aerosol and resulting in a very large increase of vapor production. Subsequently, a liquid/vapor interface (i.e. the evaporation wave front) progresses into the superheated liquid, with a velocity being some orders of magnitude smaller than the velocity of sound in the liquid.

In Fig. 1, the process, as observed by us, is shown schematically in a pressure–time diagram. At point A the liquid is in equilibrium with its vapor; at B the depressurization is initiated. After a short delay (from B to B′), the pressure decreases rapidly from B′ via C to D, because the amount of vapor flowing out of the test tube is much higher than the amount of vapor emitted by 'still evaporation' from the smooth, quiescent liquid surface. At point D the evaporation wave starts to develop at the liquid surface, which becomes unstable with droplets being torn out; the vapor production increases strongly. From D to E, the pressure in the system first continues to drop and then increases ('pressure recovery'), when the vapor production rate is now higher than the possible vapor outflow. At point E quasi-steady equilibrium between vapor production and two-phase outflow is established, and at nearly constant pressure the evaporation wave progresses with nearly constant velocity into the stagnant superheated liquid (E, F, G, H). The front of this wave appears as a convoluted,

rough, but clear interface, which separates the lower stagnant superheated liquid ('upstream') and the upper two-phase flow region ('downstream'). The two-phase flow appears to be homogeneous. With the front of the evaporation wave progressing into the superheated liquid, the internal energy of the surface layer is absorbed and the layer is cooled. This cooled liquid layer is continuously removed in form of entrained droplets in the two-phase flow, exposing always new superheated liquid to the interface. Extremely high local heat fluxes and evaporation rates do occur.

The terms used in the literature in this field are not uniform; authors use different expressions for the phenomenon that a boiling-phenomenon originates from a liquid surface instead of a solid wall. These expressions are: 'free surface boiling', 'free surface flashing' (Grolmes and Fauske, 1974); 'rapid evaporation' (Shepherd and Sturtevant, 1982); 'evaporation wave' (Chaves, 1984; Thompson et al., 1987; Frost, 1988; Shepherd et al., 1989; Hill and Sturtevant, 1989); 'surface boiling', 'boiling front', 'explosive boiling' (Reinke and Yadigaroglu, 1995). We prefer to use 'evaporation wave' as the expression widely used in literature (Meier and Thompson, 1989).

The first systematic study of evaporation waves, as far as the authors know, was performed by Grolmes and Fauske (1974) with water, methyl alcohol and refrigerants R11 and R113 as test fluids in glass tubes with 2 to 50 mm diameter. It was found that in the smaller diameter tubes a higher superheat was necessary to initiate and sustain evaporation waves.

In another study, Hill and Sturtevant (1989) succeeded in documenting photographically the mode of inception of evaporation waves from the liquid surface. They also showed that there is actually a sharp, rough interface between the superheated liquid below and the aerosol-like two-phase flow above. Their experiments were performed with R12 and R114 in a glass tube of 25.4 mm diameter with choked and unchoked outlet conditions for the two-phase flow.

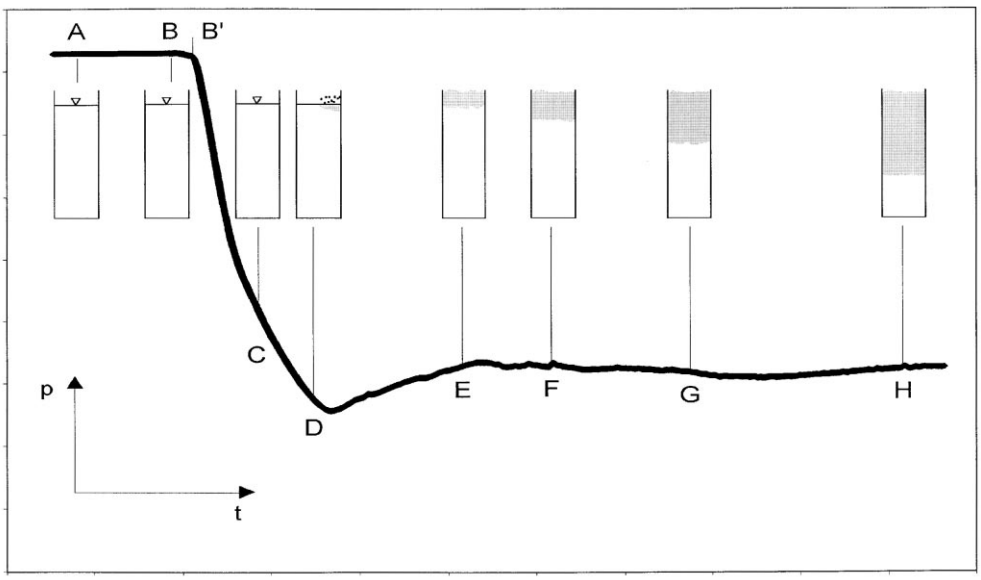

Fig. 1. Schematic description of an evaporation wave process in a pressure–time diagram.

Reinke and Yadigaroglu (1995) conducted experiments on evaporation waves with propane, butane, water and R134a in glass tubes of 25–80 mm diameter, in a funnel-shaped channel and a channel with rectangular cross section, also made of glass. They found the propagation velocity of the evaporation wave to be not related to the channel diameter and channel shape. In all these experiments, the depressurization was initiated by cutting a diaphragm over the entire cross section of the test tubes. This results in large discharge areas and in high initial depressurization rates of approximately 4000 to 12,000 bar/s.

In the present study, we investigated, whether the occurrence of evaporation waves must also be considered in 'technical systems' (e.g., liquefied-gas tanks, reactors in chemical industry), especially at lower depressurization rates with restricted discharge areas. For this purpose, flashing experiments have been performed in tubes of larger diameter than already used and in the presence of metallic elements, which should show the effect of metallic container walls.

2. Experimental set-up

The experimental facility is shown schematically in Fig. 2. The test tubes are thick-walled glass cylinders with inner diameters $d_i = 32$, 52, 102, 152 and 252 mm, arranged concentrically in a glass container with 305 mm inner diameter and 1000 mm height. The temperature of the test section is controlled by thermostated water circulating in this container. A length of around 8 cm from the bottom of the test tubes remains unheated, in order to avoid parasitic wall nucleation during depressurization from the bottom stainless steel flange. A stainless steel hose (length: 800 mm; nominal diameter: 50 mm) connects the top of the test tubes to a special ball valve. Behind the ball valve, a fast opening solenoid valve (50 mm nominal diameter) is placed and this is connected to a low pressure reservoir by another stainless steel hose (length:

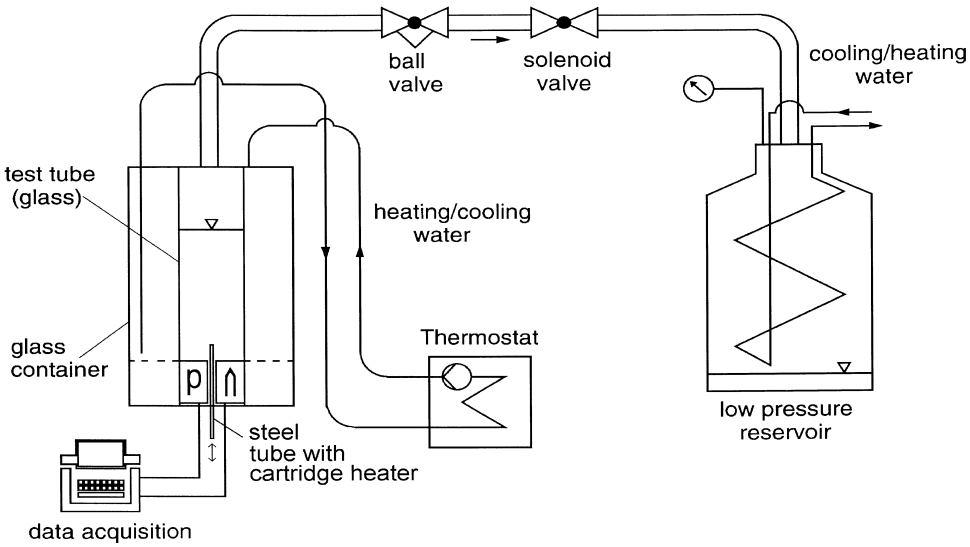

Fig. 2. Schematic drawing of the experimental set-up.

800 mm; nominal diameter: 50 mm). The low pressure reservoir is a 0.2 m^3 stainless steel container, equipped with an internal heat exchanger. The hose between experimental container and ball valve is heated electrically by a strip heater, the ball valve and the solenoid valve are heated by hot air using temperature controlled fan-forced heaters.

A 12 mm diameter stainless steel tube penetrates through the bottom flange into the test tubes. It contains an electric cartridge heater at its top and can be shifted axially upwards and downwards.

The axial temperature distribution in the test liquid is measured with a calibrated thermocouple, soldered into the top of another stainless steel tube (diameter 5 mm). This tube is also arranged in the bottom flange and can be moved up and down.

The pressure in the test tube is measured with a fast miniature pressure transducer (Kulite XTC-2-190M-VG; measuring range 1/7 bar; natural frequency $\approx$ 80 kHz), arranged in the bottom flange. The output of the transducer is recorded by a data acquisition system (Gould Windograf) with 800 samples/s. Calibration of the pressure measurement equipment showed an accuracy better than 0.03 bar. The switch-on signal of the solenoid valve and its signal for 80%-open position are recorded also by 'event markers' on the Windograf.

The pressure in the low pressure reservoir is measured with a Bourdon pressure gage (class 0.6; measuring range 1/6 bar) immediately before and after a depressurization run.

Each experimental run is recorded with a standard video-system (50 half-frames/s). In order to synchronize the video recordings and the pressure data, an illuminated diode, connected to the activation circuit of the solenoid valve, is placed in the view field of the video-camera.

The fully open ball valve provides a discharge area of $A = 334$ mm^2 with a circular cross section and can be equipped with additional laser cut seat apertures, allowing for precise control of smaller discharge areas. All discharge areas $A < 334$ mm^2 are given as equivalent cross sections, calculated on the basis of the flow coefficients supplied by the manufacturer of the valve (Worcester Controls, UK). The maximum discharge area is obtained when the ball valve is dismounted from the connection hose.

The use of a ball valve (instead of orifices) for fixing the discharge area and of a solenoid valve (instead of a diaphragm), has the advantage, that a series of experiments can be performed without exposing the interior of the experimental apparatus to ambient air. The disadvantage of this arrangement is the complicated geometric shape of the discharge cross section in the ball valve and the finite opening time ($\approx$0.05 s) of the solenoid valve. This causes unclearly defined initial conditions for the flow at the beginning of a depressurization experiment.

For the preparation of an experimental run, the test liquid (Refrigerant 11) first had to be evaporated from the low pressure reservoir and condensed in the test tube. It turned out that high condensation rates (achieved by intensive heating of the low pressure reservoir and intensive cooling of the test tube) reduced the probability of parasitic wall nucleation during the following depressurization experiment. An explanation for this effect may be, that high condensation rates result in thick liquid films quickly flowing down the glass wall and diminishing an adsorption of inert gases on the glass. Also, the time for the preparation of an experimental run decreases, resulting in a decrease of the time available for the formation of inert gas nucleation sites by diffusion. The test liquid was then heated to a temperature somewhat above the desired one by circulating temperature controlled water in the annulus

around the test tube; the guard heating of the hose to the low pressure reservoir was adjusted to prevent condensation. Using the electrical cartridge heater, the liquid was boiled intensively for around 10 min. The ball valve was adjusted to a small discharge area and the solenoid valve was opened and closed shortly for several times. These 'pre-depressurization-steps' may activate parasitic inert gas nucleation sites on the wall exhaust the available gas and thus remove them. For the actual test, the heating water temperature was adjusted to the desired initial temperature for the test liquid and, using the cartridge heater; the test liquid was boiled again at a low heat flux, in order to establish saturation pressure. The axial temperature distribution in the test liquid was measured. When the deviation from the nominal value in the heated zone, 15 cm above the bottom flange, was less than 0.3 K, the cartridge heater and the thermocouple were withdrawn into the unheated bottom zone of the test tube. The ball valve was adjusted to the desired discharge area, the video system and the data acquisition were started and the depressurization was initiated by actuating the solenoid valve.

All experiments discussed here were performed at an initial pressure (before depressurization) of $p_i = 4.3$ bar; this corresponds to an initial equilibrium temperature of $\vartheta_i = 72^\circ$C. An exception is presented in Fig. 6, where the results of experiments with $p_i = 6.7$ bar are also shown.

3. Experimental results

3.1. Glass tubes without metallic inserts

In Fig. 3(a) the experimental results for the smallest diameter test tube ($d_i = 32$ mm) and different discharge areas A are shown. The actuation of the solenoid valve is taken as $t = 0$; p is the pressure in the test tube, measured at the base of the tube. The initial pressure in the low pressure reservoir is p_R.

For all tests the initial liquid level height in the test tube is 58 ± 3 cm, which guarantees an isothermal liquid zone in the test liquid of at least 40 cm height.

During the first 0.15 s after opening the solenoid valve, the base pressure remains nearly constant in all runs. This behavior is not fully understood and can only partly be attributed to the finite opening time of the solenoid valve (0.05 s). Maybe, acceleration effects of the outflowing vapor are involved.

In the test-run with the very small discharge area $A \approx 1.5$ mm^2, the liquid level remains smooth and quiescent, emitting vapor only in 'still evaporation', and without the inception of an evaporation wave. Schlieren patterns below the liquid level indicate that heat is fed to the liquid–vapor interface by natural convection.

With the discharge area of $A = 12$ mm^2, initially also 'still evaporation' occurs on the liquid surface at a very small average depressurization rate $\Delta p/\Delta/t \approx 1$ bar/s. After $t \approx 3.6$ s an evaporation wave originates at $p_{min} = 1.35$ bar and continues to penetrate downwards into the superheated liquid, with the pressure increasing again.

For the larger discharge area $A = 21$ mm^2, an evaporation wave originates at $p_{min} = 1.3$ bar; a quasi-steady equilibrium between vapor production and two-phase outflow is established at a

pressure of $p_w \approx 1.5$ bar. We define this pressure as 'wave pressure p_w' as an average, nearly constant, pressure existing with an evaporation wave.

For the largest discharge area $A > (\pi/4)d_i^2 = (\pi/4)\ (32\ \text{mm})^2 \approx 804\ \text{mm}^2$ (when the ball valve was removed), the evaporation wave originates after $t \approx 0.4$ s at $p_{min} \approx 1.0$ bar, the depressurization rate being $\Delta p/\Delta t \approx 8$ bar/s. The superheat for the inception of the wave is $\Delta\vartheta_{max} \approx 48$ K.

The superheat $\Delta\vartheta = \vartheta_i - \vartheta_t$ is defined as the temperature difference between the initial saturation temperature in the pressurized test tube $\vartheta_i = \vartheta_{sat}(p_i)$ and the instantaneous saturation temperature $\vartheta_t = \vartheta_{sat}(p)$ at the instantaneous pressure p in the test tube. The superheat for the inception of the wave is defined as $\Delta\vartheta_{max} = \vartheta_i - \vartheta_{sat}(p_{min})$.

For $A > 804\ \text{mm}^2$, the wave pressure and consequently superheat of the bulk liquid remain

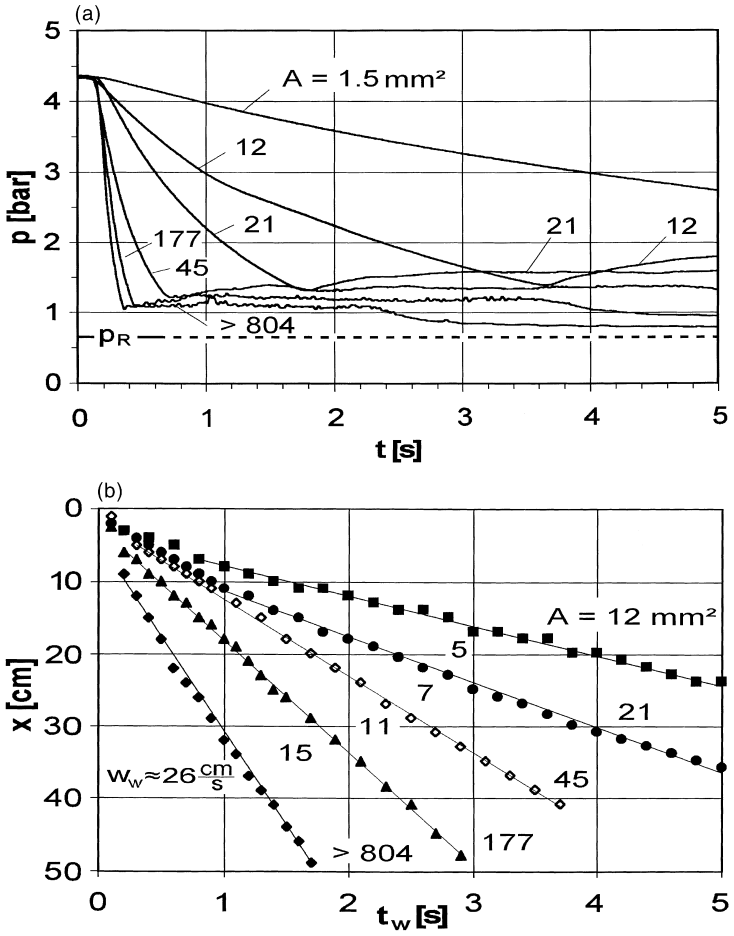

Fig. 3. (a) Pressure traces for the 32 mm diameter test tube with discharge area A as parameter (initial pressure $p_i = 4.3$ bar, reservoir pressure $p_R = 0.7$ bar). No metallic insert. (b) Evaporation wave front position vs. time for the tests of Fig. 3(a) (time since start of evaporation wave t_w; evaporation wave velocity $W_w = \Delta x/\Delta t_w$).

nearly constant until $t \approx 2.3$ s, then the evaporation wave enters the unheated bottom liquid of the test tube and dies off.

As can be seen in Fig. 3(a), for increasing discharge areas higher depressurization rates $\Delta p/\Delta t$ occur and the inception of the evaporation wave begins sooner and at somewhat lower pressures $p_{\min}$ (i.e. at higher superheats $\Delta\vartheta_{\max}$, since the theoretical equilibrium temperature $\vartheta_t(p_{\min})$ will be lower).

In Fig. 3(b) the position of the evaporation wave front in the test tube is shown for the tests of Fig. 3(a). Position $x = 0$ cm corresponds to the initial liquid level, the zero point for time t_w corresponds to that moment, when the evaporation wave starts to progress at the surface (e.g. $t_w = 0$ at $t = 3.6$ s for $A = 12$ mm^2). From this figure, the average propagation velocity of the wave front is found to be in the range of $\Delta x/\Delta t_w = 23$ cm/5 s $\approx$ 5 cm/s ($A = 12$ mm^2) to 30 cm/s ($A > 804$ mm^2).

In the tests ($A = 12$, 21, 45 mm^2) with small evaporation wave velocities ($w \leq 11$ cm/s), Schlieren patterns in the liquid below the front of the evaporation wave indicate density differences between the superheated bulk liquid and the colder liquid at the front of the evaporation wave. This means that the two-phase flow cannot remove the cooled liquid totally from the front of the evaporation wave.

As can be seen in Fig. 3(a), the small fluctuations in the pressure traces during the life-span of the evaporation waves become more pronounced for increasing discharge areas A (i.e., decreasing wave pressures p_w; increasing superheats $\Delta\vartheta$; increasing wave propagation velocities). In order to find out, whether these pressure fluctuations result from the evaporation wave front itself or from choking phenomena in the ball valve, an additional series of experiments was performed. Here, the ball valve was kept fully open ($A = 334$ mm^2) but the reservoir pressure was varied in the range $0.7 \leq p_R \leq 1.8$ bar.

Fig. 4(a) and (b) show the results of these experiments (five tests). For the highest reservoir pressure $p_R = 1.8$ bar and (for $t > 0.4$ s) a corresponding superheat of the test liquid of $\Delta\vartheta = \vartheta_i - \vartheta_{sat}(p) \approx \vartheta_i - \vartheta_{sat}(p_R) \approx 31$ K, no evaporation wave appears; the liquid level remains in 'still evaporation' for approximately 70 s (only 5 s shown in Fig. 4(a)), then a parasitic nucleation site is activated at the wall of the test tube. For $p_R \leq 1.7$ bar ($\Delta\vartheta \geq 33$ K) evaporation waves are observed. Again, the fluctuations in the pressure traces are larger for the lower wave pressures p_w and higher wave propagation velocities.

With respect to the aforementioned question about the origin of the pressure fluctuations a comparison of Figs. 3(a) and 4(a) shows that the pressure trace for the discharge area $A = 45$ mm^2 and a wave pressure of about $p_w = 1.3$ bar lies just in between those for the reservoir pressures $p_R = 1.3$ and 1.1 bar (in Fig. 4(a)), but here, the discharge area is about seven times larger with $A = 334$ mm^2. From Fig. 4(b) it can be concluded that the flow for $p_R = 1.3$ and 1.1 bar is not choked in the discharge area: when the reservoir pressure is further reduced to $p_R = 0.7$ bar, the propagation velocity of the evaporation wave still increases (from $w \approx 11$ cm/s at $p_R = 1.1$ bar, to $w \approx 17$ cm/s), thus, a higher mass flux occurs in the discharge area and the flow is not choked. For the $A = 45$ mm^2 test, the pressure ratio in the discharge area is approximately $p_R/p_w \approx 0.7/1.3 < 0.55$, indicating that the two-phase flow in the discharge area might be choked (according to Leung, 1986). All three tests ($A = 45$ and 334 mm^2 with $p_R =$ 1.3 and 1.1 bar), however, show similar pressure fluctuation patterns. This seems to indicate that these higher frequency pressure fluctuations (which also have been observed in the

experiments by Grolmes and Fauske, Hill and Sturtevant, Reinke and Yadigaroglu) do not result from any downstream choking but rather from the evaporation front itself.

Visual observations during the experiments and close inspection of the video recordings show, that the macroscopic shape of the liquid/two-phase interface is convex for low propagation velocities and tends to become concave for high velocities. Concave wave fronts (looked at from the two-phase side, i.e. from above) have been observed also by Hill and Sturtevant and by Reinke and Yadigaroglu. A concave shape of the front indicates, that the propagation of the wave is dominated by phenomena occurring in the center of the tube ('far-wall phenomena'), whereas a convex shape indicates the dominance of phenomena originating at the wall ('near-wall phenomena').

In Fig. 5 some pressure traces are shown for the largest diameter test tube ($d_i = 252$ mm) and for different initial liquid level heights h. The discharge area ($A = 334$ mm^2) and the reservoir pressure ($p_R = 0.7$ bar) were kept constant.

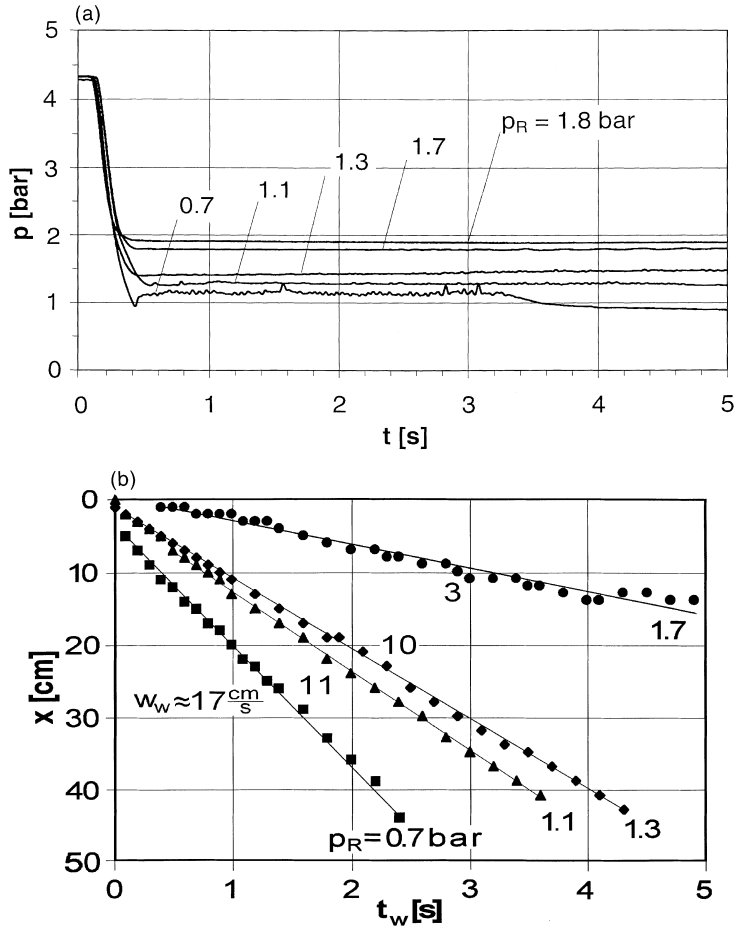

Fig. 4. (a) Pressure traces for the 32 mm diameter test tube with reservoir pressures p_R as parameter ($A = 334$ mm^2). No metallic insert. (b) Evaporation wave front position vs. time for the tests of Fig. 4(a).

The depressurization rates $\Delta p/\Delta t$ are smaller for the small heights, since for a small liquid height the initial expandable vapor volume in the test tube is large.

The dashed parts of the pressure traces of tests $h = 500$, 581 and 656 mm indicate the appearance of a parasitic wall nucleus; these occurred in the majority of the experiments with the largest test tube. Data shown are for testruns, where wall nucleation (if ever) occurred only after the inception of an evaporation wave at the liquid surface. Close inspection of the video recordings of these runs shows, that nearly always only one single bubble (not a bubble chain) grew somewhere from the wall. This may reveal that these 'nucleation sites' are accidental agglomerations of inert gas, precipitated from the test liquid. It should be mentioned that for the high superheat $\Delta\vartheta = 46$ K, even sites with critical radii as low as $r_c \approx 75$ nm can be activated (according to $r_c = 2\sigma/\Delta p$). The probability for the presence of such sites increases with the size of the wetted wall area and the length of the depressurization time. As can be observed from the pressure traces in Fig. 5, the nucleation of a single bubble on the container wall (dashed curves) results in a steeper and higher pressure recovery, than the occurrence of an evaporation wave from the liquid level ($h = 620$ and 624 mm). The video recordings show, that such a single bubble grows within approximately 0.5 s to diameters of ≈ 200 mm, occupying nearly the entire cross section of the test tube. The initially smooth liquid/vapor interface of the bubble becomes disturbed and rough for bubble diameters greater than 50–100 mm. This may indicate the inception of evaporation wave-like transport phenomena now appearing at the *bubble's* interface (Barthau and Hahne, 1996). The growth and rise of this vapor mass results in a strong internal circulation of the superheated liquid in the test tube and, therefore, in a strongly increased vapor production.

The good reproducibility of the minima of the pressure traces in Fig. 5 — which indicate the inception of evaporation waves — is attributed to the fact, that the interior of the experimental set-up was not exposed to ambient air. For the sake of clarity only 6 of the 13 runs for level heights $500 \leq h \leq 705$ mm are shown, the pressure minimum being for all 13 runs $p_{min} = 1.12 \pm 0.04$ bar, corresponding to a superheat $\Delta\vartheta_{max} = 46 \pm 1$ K.

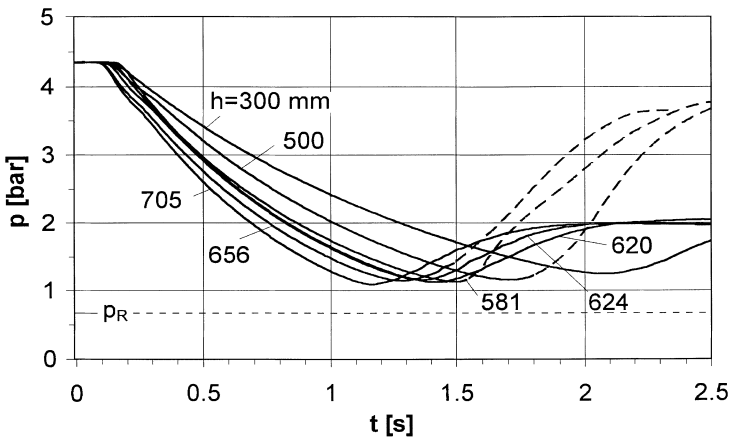

Fig. 5. Pressure traces for the 252 mm diameter test tube with initial liquid level height has parameter ($p_R = 0.7$ bar; $A = 334$ mm^2). No metallic insert.

In Fig. 6 the superheats $\Delta\vartheta_{max} = \vartheta_i - \vartheta_{sat}(p_{min})$ for the inception of evaporation waves are summarized for different test tube diameters; with $p_i = 4.3$ and 6.7 bar being the initial pressures of the saturated liquid. As discussed for Fig. 3(a), $\Delta\vartheta_{max}$ also depends on the depressurization rate $\Delta p/\Delta t$; therefore, the data are shown for the highest and the lowest $\Delta p/\Delta t$ common to all runs with different diameter test tubes. The experiments with the different diameter tubes have been conducted in the sequence $d = 52$, 152, 32, 252, 102 and 32 mm over a period of approximately 2 years and the test fluid has been evaporated and condensed more than 100 times during this period. Despite of some earlier results for the 32 mm test tube showing higher superheats than the later ones, it is felt that the whole data set is superimposed by a small 'time and/or purity effect', which caused higher $\Delta\vartheta_{max}$ at later experiments. Taking this into account, it is concluded from the results of the present experiments with R11, that a consistent influence of the test tube diameter on the superheat $\Delta\vartheta_{max}$ for the inception of evaporation waves is non-existent or rather weak for diameters $30 \leq d \leq 250$ mm.

The shaded zone for $2 \leq d \leq 50$ mm in Fig. 6 represents the experimental results of Grolmes and Fauske for R11 with an initial pressure of $p_i \approx 1.3$ bar and very low reservoir pressures of $p_R < 0.02$ bar. The upper boundary of the shaded zone corresponds to the superheat where evaporation waves originated and continued to penetrate into the superheated liquid; below the lower boundary of the zone, only 'still evaporation' occurred at the liquid surface.

A comparison with the Grolmes/Fauske data is difficult, due to different definitions of the superheat $\Delta\vartheta_{max}$. Whereas in the present study the superheat is taken as $\Delta\vartheta_{max} = \vartheta_i - \vartheta_{sat}(p_{min})$, with p_{min} as the pressure measured in the test tube, Grolmes and Fauske evaluate $\Delta\vartheta_{max} = \vartheta_i - \vartheta_{sat}(p_x)$ with p_x as the 'reservoir pressure after rapid depressurization'. It may be possible, that the higher superheats for the smaller test tube diameters in the Grolmes/Fauske data set, can be explained on the basis of the Borda–Carnot relations (pressure drop in sudden cross-section area enlargements, see e.g., Truckenbrodt, 1968).

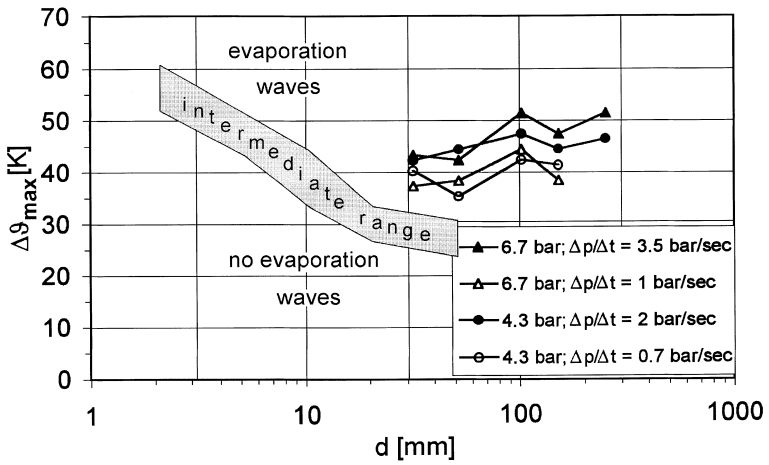

Fig. 6. Superheat $\Delta\vartheta_{max}$ for the inception of evaporation waves vs. test tube diameter d with initial pressure p_i and depressurization rate $\Delta p/\Delta t$ as parameter. No metallic insert. Shaded area: experimental results of Grolmes and Fauske.

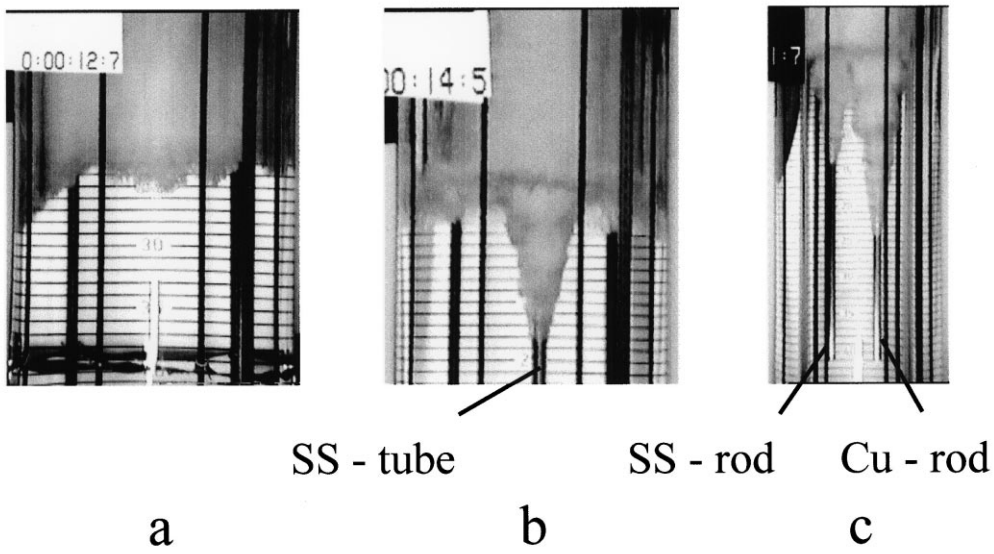

Fig. 7. Evaporation waves without and with metallic inserts in the test tube, (a) 252 mm diameter test tube without metallic inserts; (b) 252 mm diameter test tube with stainless steel insert, and (c) 152 mm diameter test tube with stainless steel insert (left) and copper insert (right).

3.2. Glass tubes with metallic inserts

In order to simulate the effect of metallic container walls on the inception and propagation of evaporation waves, metallic inserts were arranged in the test tubes with diameter $d = 152$ and 252 mm. In one series of experiments, the 12 mm diameter stainless steel tube, containing the cartridge heater (not heated in this case), was shifted upward in the 152 mm and in the 252 m test tube, to penetrate through the liquid surface. In another series, two rods, one made of stainless steel and one of copper (diameter = 10 mm), were arranged in the 152 mm diameter test tube, also penetrating through the liquid surface.

In most depressurization runs, evaporation waves originated from the circumference of the metal rods where the liquid surface touches these rods (solid/liquid/vapor contact). From there, boiling progressed down the rods into the superheated liquid. From the metal rods, boiling spreads out in a cone-shaped form as shown in Fig. 7(b) and (c).

Fig. 7(a) shows an evaporation wave in the 252 mm test tube without metallic inserts,[1] while Fig. 7(b) gives the cone-shaped boiling form on the stainless steel (SS) insert, in the same test tube. This form develops since the propagation velocity of the vapor/liquid front along the metallic surface is higher than its propagation velocity in the liquid, i.e., the propagation is governed by 'near-wall phenomena'.

Fig. 7(c) shows the stainless steel rod (left) and the copper rod (right) in the 152 mm test tube. Here, boiling originated first on the copper rod, the propagation velocity is higher on

[1] The vertical black lines in Fig. 7 are outside through bolts holding the flanges together.

copper than on steel. Very rarely, heterogeneous nucleation occurred in the lower part of the bulk liquid on the metallic surfaces. With respect to the initial conditions, used in many flashing models (cf. Section 1), this was a very unexpected result.

Fig. 8 gives the pressure traces for the 152 mm test tube with the stainless steel and the copper rod for different discharge areas A. For comparison, also shown are the positions of the pressure minima for the corresponding experimental runs without metallic inserts (dash-dotted line) and with the single stainless steel tube (dashed line). As can be seen from the position of the pressure minima (dotted line and dashed line), boiling on metallic inserts starts at higher pressures (i.e. at lower superheats) than evaporation waves in glass tubes without metal inserts (dash-dotted line).

When boiling spreads along the metal rods into the superheated liquid, the cone-shaped liquid/two-phase interface is larger than the interface in the runs without metallic inserts (Fig. 7), thus, more vapor is produced and we have a higher pressure recovery. On the other hand, a higher pressure recovery (i.e. higher wave pressure p_w) gives a smaller superheat of the metastable liquid and, therefore, reduces parasitic wall nucleation. This means a self-limitation of the front propagation velocity and a self-protection of the wave process.

4. Discussion

Only few studies deal with phenomena on propagating vapor fronts during flashing processes. Concerning the *inception* of evaporation waves, Hill and Sturtevant note: "At the highest superheats, individual nucleation sites rapidly initiate at random spots on the liquid free-surface and at the glass/liquid contact line.... At intermediate superheats, nucleation begins only at many sites on the glass/liquid contact line.... At low superheats, nucleation begins at one or more sites on the glass/liquid contact line and propagates across the surface."

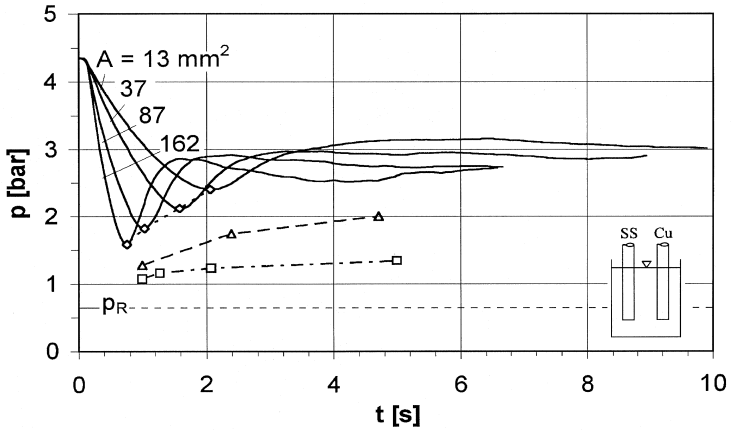

Fig. 8. Pressure traces for the 152 mm diameter test tube with two metal rods (stainless steel, copper) with discharge area A as parameter. Position of pressure minima: ◇ two metal rods (SS, Cu); △ single stainless steel tube; □ without metallic inserts.

It is exactly this 'low superheat mode' which we have observed in the present study at much smaller depressurization rates than Hill and Sturtevant.

As can be concluded from the experimental results for $\Delta\vartheta_{max}$ presented in Fig. 6, the inception of the liquid surface instability (e.g. tear out of droplets, Fig. 1, point D) on the glass/liquid contact line, as a statistical nucleation process, seems — if at all — only weakly related to the length of this contact line $d \cdot \pi$. One might expect, that a longer contact line provides a higher probability for the occurrence of a 'most favorable' nucleation site, than a smaller. Nucleation therefore should start at a lower superheat. Comparing the 252 mm diameter tube with the 32 mm, the difference in length of the contact line is about an order of magnitude, but the superheat $\Delta\vartheta_{max}$ in Fig. 6 for the great length is even somewhat higher than for the small length. Since data presented in Fig. 6 have been evaluated for constant depressurization rates $\Delta p/\Delta t$ (corresponding to $\Delta\vartheta/\Delta t$) for the different diameter tubes, the superheat–time relation $\Delta\vartheta/\Delta t$ (and with $\Delta p \approx$ const. the 'age' of the contact line) for the different contact lines ($d \cdot \pi$) is also the same.

Since, for the different diameter tubes, nucleation appears to be not influenced by contact length and since the depressurization time is the same, we conclude, that the nucleation process on the glass/liquid contact line is not dominated by stochastic effects, depending, e.g., on statistically distributed nucleation per length and time, at least in the range of nominal superheats $35\ \mathrm{K} \leq \vartheta \leq 50\ \mathrm{K}$.

The fact, that in the experiments with metallic inserts, boiling always originates at lower superheats, compared to glass, from the much shorter metal/liquid contact line, indicates, that metal/liquid contact lines — compared to glass/liquid — either offer a better deterministic nucleation behavior, or/and a higher local superheat in the meniscus region. The term 'deterministic nucleation' here refers to macroscopic influence on nucleation such as surface roughness, contact angles, gas pockets... (cf. Alamgir and Lienhard, 1981).

As can be seen in Fig. 8, the inception superheat is lowest when the stainless steel and copper rod are together in the test tube, for stainless steel alone it is higher and it is highest for glass. The SS–Cu arrangement is governed by the copper rod in its inception behavior, as discussed in Fig. 7(c). While the differences in the inception superheat can be explained by different deterministic nucleation behavior alone, the fact, that in each of the three series of Fig. 8, the inception superheat decreases with increasing inception time, i.e., the time increment from pressure release ($t = 0$) until reaching the minimum pressure ($t = t_i$), requires additional explanation.

The superheat $\Delta\vartheta_{max}$ defined and discussed in the preceding sections, always refers to the *bulk* liquid state in the test tube. In reality, the inception of boiling in the solid/liquid contact region is governed by the *local* superheat in this region. As discussed in Fig. 1, in the very initial stage of depressurization 'still evaporation' occurs on the liquid surface which is cooled down. The heat transport to this surface is governed by unsteady heat conduction in the liquid. On the brim, however, where the evaporating liquid film, adjacent to the solid wall, becomes continuously thinner, the shape, curvature and local superheat of the film may be affected by unsteady conduction in the solid wall. Thus, the thermal properties of the wall material (thermal conductivity, specific heat capacity, density) may play the dominant role for the inception of boiling.

It is interesting to note the statement by Grolmes and Fauske (1974) in the discussion of

their paper: "...Upon depressurization, the tube wall provides a line heat source as the liquid cools by evaporation. In this regard, we would not be surprised to find that thermal properties of the tube wall, as well as diameter, also influence the transition from evaporation to flashing...".

The quasi-steady *propagation* of evaporation waves (at constant wave pressure) in small diameter glass tubes ($d_i \leq 52$ mm) has been found to be governed by either of two different modes:

1. At high depressurization rates, the shape of the liquid/two-phase interface (the wave front) was observed to be concave. This indicates that the propagation process is governed by 'far-wall phenomena', which depend only on the thermodynamic and transport properties of the fluid. This propagation mode has been also observed by Hill and Sturtevant, Reinke and Yadigaroglu.
2. At low depressurization rates, the shape of the liquid/two-phase interface appeared as being convex, indicating the propagation is governed by 'near-wall phenomena'. Taking into account the observations with metallic inserts, where boiling occurred on the metal wall, these 'near-wall phenomena' can be identified as boiling on glass.

It is somewhat puzzling to observe for glass that, at high depressurization rates, the velocity of the evaporation wave front in the center of the tube is higher than that for boiling along the wall, whereas at low $\Delta p/\Delta t$ the opposite is true.

The propagation of evaporation waves in the larger test tubes ($d_i = 102$, 152 and 252 mm) has been studied only at very low depressurization rates. Here, the shape of the wave front is highly irregular, it is neither concave nor convex; the front proceeds sometimes along the glass wall downwards, but mostly 'fingers' from the liquid surface downwards into the superheated liquid. Schlieren patterns in the superheated liquid below the wave front indicate, that the upward two-phase flow cannot totally remove the cooled liquid from the front. With metallic inserts, no fingering from the liquid surface is observed, but boiling only propagates downwards along the metallic surface.

As was observed in the experiments of Fig. 7, the boiling velocity down the copper rod is higher than that down the stainless steel, and this is still higher than that down the glass. It may be that the propagation velocity is influenced somewhat by the surface roughness (both metal rods were finished with the same size emery paper), but — as mentioned before — we do think, that boiling down a wall strongly depends on the thermal properties of the wall material (especially its thermal diffusivity).

It is interesting to note, that the boiling phenomena on the metallic inserts observed in the present study of adiabatic flashing processes, strongly resemble boiling propagation observed in experiments, dealing with boiling inception at high superheats on heated test sections (Avksentyuk and Ovchinnikov, 1993; Fauser and Mitrovic, 1996).

On the basis of direct visual observations and close inspection of the video-recordings, the downstream *two-phase flow pattern* of an evaporation wave (without and with metallic inserts) can be classified in the frame of two-phase flow terminology as homogeneous (cf. Fig. 7). However, the higher frequency pressure fluctuations discussed in Section 3.1 indicate, that the flow is not strictly homogeneous (at least near the wave front). This has been observed and discussed also by Hill and Sturtevant.

Without direct evidence from our experiments, but taking into account the formation of the two-phase flow at the interface (wave front), there are very good reasons to assume, that vapor is the continuous phase with entrained liquid droplets as the dispersed phase: the vapor, originating from the wave front, first has to accelerate the liquid droplets and then has to carry them upward against gravity. This requires the occurrence of slip.

Further, it might be worth mentioning that most probable the liquid droplets in the two-phase flow are still superheated with respect to the actual pressure in the container, i.e. the two-phase flow is not in thermal equilibrium.

5. Summary

The results of the present experimental study can be summarized as follows:

- Adiabatic flashing of a highly wetting liquid (Refrigerant 11) in glass containers is apt to result in evaporation waves. We observed a rather homogeneous downstream two-phase flow with vapour as the continuous phase and liquid droplets as the dispersed phase.
- Evaporation waves occur also in larger diameter systems (at least up to $d = 250$ mm), the superheat for the inception being (nearly) independent of the diameter.
- Evaporation waves can originate also at low depressurization rates (down to $\Delta p/\Delta t \approx 1$ bar/s).
- Metallic inserts, within the superheated liquid, promote the inception of boiling, resulting in evaporation waves with large liquid/two-phase interfaces. It is likely, that boiling fronts originate in metallic containers also from the liquid surface contact line.
- Front-like phenomena (evaporation waves and boiling) should be taken into account in modelling of flashing processes, supplementing the assumptions of homogeneous or heterogeneous nucleation as the main source of vapour/liquid interface.

Acknowledgements

This experimental investigation was supported by the Deutsche Forschungsgemeinschaft, im Schwerpunktprogramm 'Transiente Vorgange in mehrphasigen Systemen mit einer oder mehreren Komponenten'. The test liquid was supplied by Hoechst company. The authors gratefully acknowledge this support.

References

Akyuzlu, K.M., 1993. A parametric study of boiloff initiation and continuous boiling inside a cryogenic tank using a one-dimensional multi-node nonequilibrium model. Phase Change Heat Transfer, ASME, HTD-262, 1993, pp. 9–14.

Alamgir, Md., Lienhard, J.H., 1981. Correlation of pressure undershoot during hot-water depressurization. J. Heat Transfer 103, 52–55.

Avksentyuk, B.P., Ovchinnikov, V.V., 1993. A study of evaporation structure at high superheatings. Russian J. Engineering Thermophysics 3, 21–39.

Bartak, J., 1990. A study of the rapid depressurization of hot water and the dynamics of vapour bubble generation in superheated water. Int. J. Multiphase Flow 16, 789–798.

Barthau, G., Hahne, E., 1996. Fragmentation of a vapour bubble growing in a superheated liquid. EUROTHERM Sem. No.48: Pool Boiling 2. Paderborn, Germany, pp. 105–110.

Boesmans, B., Berghmans, J., 1994. Non-equilibrium vapour generation rate and transient level swell during pressure relief of liquefied gases. In: Tenth Int. Heat Transfer Conf., vol. 3, Brighton, 281–286.

Chaves, H., 1984. Phasenübergänge und Wellen bei der Entspannung von Fluiden hoher spezifischer Wärme. Mitt. Max-Planck-Institut f. Strömungsforschung Nr 77.

Deligiannis, P., Cleaver, J.W., 1992. Determination of the heterogeneous nucleation factor during a transient liquid expansion. Int. J. Multiphase Flow 18, 273–278.

Deligiannis, P., Cleaver, J.W., 1996. Blowdown from a vented partially full vessel. Int. J. Multiphase Flow 22, 55–68.

Elias, E., Chambre, P.L., 1993. Flashing inception in water during rapid decompression. J. Heat Transfer 115, 231–238.

Fauser, J., Mitrovic, J., 1996. Heat transfer during propagation of boiling fronts in superheated liquids. Eurotherm Seminar No.48: Pool Boiling 2. Paderborn, Germany, pp. 283–290.

Frost, D.L., 1988. Dynamics of explosive boiling of a droplet. Phys. Fluids 31, 2554–2561.

Grolmes, M.A., Fauske, H.K., 1089. Axial propagation of free surface boiling into superheated liquids in vertical tubes. Fifth Int. Heat Transfer Conf., Tokyo, vol. 4, pp. 30–34; vol. 7, p. 99.

Hill, L.G., Sturtevant, B., 1989. An experimental study of evaporation waves in a superheated liquid. In: IUTAM Symp. on Adiabatic Waves in Liquid–Vapor Systems, Göttingen, Germany, 25–37.

Kendoush, A.A., 1989. The delay time during depressurization of saturated water. Int. J. Heat Mass Transfer 32, 2149–2154.

Leung, C.J., 1986. A generalized correlation for one-component homogeneous equilibrium flashing choked flow. AIChE J. 32, 1743–1746.

Lund, K., 1986. Druckentlastung von mit Flüssigkeit befüllten Apparaten. Diss. Univ. Hannover, Germany.

Meier, G.E.A., Thompson, P.A. (Eds.). Adiabatic waves in liquid–vapor systems. IUTAM Symp. on Adiabatic Waves in Liquid–Vapor Systems, Göttingen, Germany, 1989. Springer-Verlag, Berlin.

Reinke, P., Yadigaroglu, G., 1995. Surface boiling of superheated liquids. Two-Phase Flow Modelling and Experimentation, Rome, vol. 2, 1155–1162.

Shepherd, J.E., Sturtevant, B., 1982. Rapid evaporation at the superheat limit. J. Fluid Mech. 121, 379–402.

Shepherd, J.E., McCahan, S., Cho, J., 1989. Evaporation wave model for superheated liquids. In: IUTAM Symp. on Adiabatic Waves in Liquid–Vapor Systems, Göttingen, Germany, 3–12.

Thompson, P.A., Chaves, H., Meier, G.E.A., Kim, Y.G., Speckmann, H.D., 1987. Wave splitting in a fluid of large heat capacity. J. Fluid Mech. 185, 385–414.

Truckenbrodt, E. 1968. Strömungsmechanik. Springer-Verlag, Berlin, p. 218.

Viecenz, H.J., 1980. Blasenaufstieg und Blasenseparation in Behältern bei Dampfeinleitung und Druckentlastung. Diss. Univ. Hannover, Germany.